The Calibration of AVHRR visible dual gain using Meteosat-8 for NOAA-16 to 18

David R. Doelling[*a] , Donald P. Garber[b], L. A. Avey[a], Louis Nguyen[b], Patrick Minnis[b]

[a]Science Systems and Applications, Inc., One Enterprise Pkwy Ste 200, Hampton, VA 23666 USA
[b]NASA Langley Research Center, 21 Langley Blvd MS 420, Hampton, VA 23681-2199 USA

david.r.doelling@nasa.gov; phone 1.757.827.4634; http://www-pm.larc.nasa.gov

ABSTRACT

The NOAA AVHRR program has given the remote sensing community over 25 years of imager radiances to retrieve global cloud, vegetation, and aerosol properties. This dataset can be used for long-term climate research, if the AVHRR instrument is well calibrated. Unfortunately, the AVHRR instrument does not have onboard visible calibration and does degrade over time. Vicarious post-launch calibration is necessary to obtain cloud properties that are not biased over time. The recent AVHRR-3 instrument has a dual gain in the visible channels in order to achieve greater radiance resolution in the clear-sky. This has made vicarious calibration of the AVHRR-3 more difficult to unravel. Reference satellite radiances from well-calibrated instruments, usually equipped with solar diffusers, such as MODIS, have been used to successfully vicariously calibrate other visible instruments. Transfer of calibration from one satellite to another using co-angled, collocated, coincident radiances has been well validated. Terra or Aqua MODIS and AVHRR comparisons can only be performed over the poles during summer. However, geostationary satellites offer a transfer medium that captures both parts of the dual gain. This AVHRR-3 calibration strategy uses, calibrated with MODIS, Meteosat-8 radiances simultaneously to determine the dual gains using 50km regions. The dual gain coefficients will be compared with the nominal coefficients. Results will be shown for all visible channels for NOAA-17.

Keywords: Vicarious Calibration, AVHRR3, Meteosat, Visible, Dual Gain.

1. INTRODUCTION

The Advanced Very High Resolution Radiometer (AVHRR) instrument onboard the National Oceanic and Atmospheric Administration (NOAA) have been operational for over almost continuously for 25 years. The AVHRR radiances have been incorporated into vegetation index, aerosol, land classification, and cloud property products. These products are dependent on the AVHRR calibration used. All AVHRR IR channels have onboard blackbodies that provide accurate IR temperatures. However, the AVHRR instrument has no onboard calibration in the visible and is known to degrade over time. AVHRR derived parameters need to be consistent over multiple platforms to observe long-term trends. Reliable calibration of AVHRR radiances is key to study climate change from AVHRR products. It should be noted that the NOAA satellites ending with NOAA-15 were in orbits that were allowed to drift over time, thus requiring diurnal normalization of AVHRR product parameters. The AVHRR/3 NOAA platforms have stabilized orbits beginning with NOAA-16. The nominal or pre-launch calibration is given at the NOAA POD or KLM User's Guide (http://www.ncdc.noaa.gov/oa/pod-guide/ncdc/docs/intro.htm). There have been many published post-launch AVHRR calibration coefficients derived by vicarious calibration. These include, stable desert (Rao and Chen. 1999) and polar ice (Loeb 1997) targets, congruent aircraft calibration (Abel and Guenther 1993.), inter-calibration of satellites with onboard calibration (Doelling et al 2004, Heidinger et al. 2002, Nguyen et al. 2004) and deep convective clouds as stable bright target (Doelling et al. 2004). The degradation of the visible sensors is greatest following launch and tapers off after a few years. There are two general methodologies to transfer calibration from one instrument to another using ray-matched coincident and collocated radiances. One relies on spatial pixel-matched radiances, where both instruments have the same nominal pixel resolution, thus requiring good navigation on both satellites. For this method, usually only the nadir pixel is considered, such as the Simultaneous Nadir Overpass (SNO) method. The second method relies on spatially matching large field of views (FOV) covering many pixels to mitigate navigation and time difference errors due to advection. Larger FOV also guarantees spatial consistency and significantly reduces the standard error of the resultant regression. Wielicki et al. 2007 shows a factor of three reduction in the standard error from using a FOV of 25km to 100km. This method has been tested with many satellite pairs and consistency between well-calibrated visible sensors (Minnis et al 2001 and Minnis et al. 2007a). Larger FOV do not require both imagers to have the same nominal

pixel resolution. The upcoming Climate Absolute Radiance and Refractivity Observatory (CLARREO) mission goal is to calibrate all operation sensors by using hyper-spectral instruments and requires a nominal footprint of 100 km (Wielicki et. 1007). The aim of the CLARREO mission is calibrate all imager regardless of spectral response functions. Spectral normalization of the visible sensors needs to be addressed regardless of method. The author notes that even under the best of ray-matching conditions of VIRS and Terra 0.65µm imagers using nadir only, 100km FOV, 3 minute, and spatial uniformity restrictions, the visible standard error of the regression was 4.6%, whereas the IR standard error was 0.2%.

With the advent of the AVHRR/3 instrument (beginning with NOAA-15) the visible channels were designed with dual gains (http://www.ncdc.noaa.gov/oa/pod-guide/ncdc/docs/klm/html/c7/sec7-1.htm). Essentially the low radiance gain has twice the sensitivity of the high gain. The dual gain cross-over point is determined before launch along with the nominal dual gain calibration using integrating spheres and lamps. The dual-gain was implemented to enhance the radiometric resolution for low radiances, to increase sensitivity in AVHRR clear-sky products such as the vegetation index. This had the unintended consequence of complicating vicarious calibration techniques to monitor the visible calibration over time. For example the deep convective clouds technique (DCCT) uses cold bright TOA targets, which produce consistent albedos (Hu et al 2004), can only monitor the stability of the high gain over time. Stable bright desert targets and the moon are only detected in the low radiances. Using Moderate-Resolution Imaging Spectroradiometer (MODIS) to calibrate AVHRR using coincident ray-matched radiances can only be achieved where the two polar orbiters ground intersects are located. These are located at 70° N or 70° S. At 70° N the local time of the matches is near local noon. On June 23 the solar zenith angle is 45°, limiting the duration of which the upper gain can be calibrated with MODIS to ~ 2 months out of the year and the highest counts are limited to 650 due to polar matching. Heidinger et al 2001, using the first method, used near nadir pixels from both NOAA-16 AVHRR and Terra-MODIS from two ground intersects. The coincident ground intersects were limited by the availability of AVHRR HRPT (1km nominal resolution) scheduled data, only two images were considered, since MODIS also has a 1km nominal resolution. Since pixel radiances were matched within 10° viewing angle, the AVHRR pixels where remapped onto the MODIS pixels to mitigate any navigational errors. 28010 pixels were collocated, the dual gains were derived from the low and high gains separately. Doelling et al. 2004, using the second method using near nadir ray-matched 50km FOV. Temporally continuous AVHRR GAC (3x5 km nominal resolution) pixel radiances were used. When combining low and high gain pixel counts the counts were first converted to radiances and relying on the nominal calibration. The dual gains do not degrade linearly, especially in the 0.85 µm visible channel (Doelling et al. 2002). This limits the effectiveness of this method with dual gain sensors and reliable results were derived only when the high gain radiances were minimal.

Ideally, a single method is needed that can resolve the lower and upper gain simultaneously from the same AVHRR image over the entire range of counts, and continuously over the course of a year. Observing the dynamic range can be resolved by using a calibration transfer satellite over the equator, such as Meteosat-8, which can been calibrated using MODIS for all 3 visible (0.65, 0.86, 1.6 µm) channels. Can the dual gain calibration coefficients be derived directly using multiple FOV pixel radiances as is required for the CLARREO mission? This paper provides four mathematical approaches to resolve the dual gain, depending on whether a discontinuity is allowed at the crossover point or break point or whether the space count is set. This paper shows results for NOAA-17 and Meteosat-8 during February of 2007. This method will then be applied to NOAA-16 through 18 beginning with the operation of the Meteosat-8 imager on March 2004 to the present. If the method is reliable consistent monthly calibration coefficients will be derived. The AVHRR derived calibration coefficients can then be validated by matching NOAA-16 and 18 with MODIS and NOAA-17 with Aqua as well NOAA-16 and 17 and NOAA17 and 18 over the poles using the method of Doelling et al 2001 and 2004. All these pairs should give consistent results if the dual gain was resolved successfully.

2. METEOSAT-8/NOAA-16 TO 18 CALIBRATION METHODOLOGY

2.1 Methodology
The Meteosat-8/NOAA-17 cross-calibration is similar to the geostationary (GEO) to Low Earth Orbit (LEO) method outlined in Minnis et al 2001. All Meteosat data was obtained either real-time from (McIDAS http://www.ssec.wisc.edu/mcidas/) or historically from EUMETSAT (http://archive.eumetsat.org/en/index.html). The AVHRR data was collect in real-time from McIDAS and historically from CLASS (http://www.class.noaa.gov/saa/products/welcome). Real-time analysis started with January 2007. Meteosat-8 3-km

radiances were averaged into 0.5° latitude by longitude regions bounded by 15° N to 15° S and 15° W and 15° E. Similarly, the AVHRR GAC (3x4 km) pixel level counts were averaged into the same grid keeping the low and high gain counts separate. The AVHRR GAC pixel radiance is based on a 4 pixel HRPT scan mean skipping the 5th element and taking every 3rd line. It is uncertain whether the mean is performed in count units or radiance (Fred Wu personal communication). If the 4-pixel mean were based in counts, this would add another degree of uncertainty to the visible radiances, since the count to radiance conversion is based on the 4-pixel mean. Coincident ray-matched regions were limited by 7.5 minutes (Meteosat-8 has a 15 minutes scan cycle), ocean scenes (to avoid land spectral differences), non-glint regions, scattering angle less than 10°, relative azimuth angles between 10° and 170° to avoid direct backscatter and forward scatter. The view angle is limited by the spatial domain and is less than 30°. The cosine solar zenith angle differences were normalized as well as the solar constants and are shown in Table 1. Partial pixel sampled regions were rejected. All monthly qualifying coincident ray-matched regional radiances or counts are regressed. A spatial uniformity test was applied to the Meteosat-8 0.65μm 50-km FOV pixel radiances, restricted the standard deviation to less then 20% of the mean. The monthly gains are then plotted as a function of time to determine the gain change as a function of day since launch. No visible spectral corrections were attempted for this study.

Satellite	Launch date	Solar Constant (Wm^{-2}str^{-1}um^{-1})			AVHRR Break Point (10 bit count)		
		0.64μm	0.86μm	1.6μm	0.64μm	0.86μm	1.6μm
Met-8	Aug 28,2002	515.0	354.3	73.28			
Terra-MODIS	Dec 18,1999	508.8	316.8	75.05			
NOAA-16	Sep 21, 2000	523.4	329.3	77.5	497.5	500.3	498.7
NOAA-17	Jun 24, 2002	522.4	328.4	77.1	497.53	500.32	98.66
NOAA-18	May 20, 2005	523.0	317.7	78.0	500.54	500.40	500.56

Table 1. Provides the launch date, solar constants used in normalization, and NOAA-16 to 18 AVHRR break-points.

The Meteosat-8 counts were first converted to radiances using gains derived from December 2006 MODIS/Meteosat-8 regression based on the same GEO to LEO technique. The gains are given in Table 2. The published Meteosat-8 offset of 51 was used in this study. Note the standard error of the fits are ~5% except 0.86μm channel. These are in order of the 4.6% achieved with MODIS and VIRS and are probably the extent of the spectral differences. Note the Aqua-MODIS/NOAA-17 0.65μm standard error is 1.4% and 1.9% for September 2003 and July 2004, respectively, since the spectral response functions are nearly identical (Fig. 1a). July 2004 observed some high counts, which increased the standard error. The 0.86 μm on MODIS saturates for very high radiances and effects 50km MODIS mean FOV radiances greater the 250 Wm^{-2}str^{-1}um^{-1} and the regression was limited to that radiance. This explains the larger standard deviation of the 0.86μm channel. Note the Aqua/NOAA-17 0.86μm standard error is a factor of 2.5 times the 0.65μm, due to the saturation. For channels 0.65μm and 1.6μm the EUMETSAT March 2007 gains are within 1%, after correcting for the spectral difference (0.9741 Minnis et al. 2007b) over ocean for the 0.65μm channel. The 0.86μm channel difference is 14% and in part due to the saturation of the MODIS channel, but more than likely spectral (Fig. 1b), though it seems rather large.

Satellite Pair	Terra-MODIS/Meteosat-8		EUMETSAT	Aqua-MODIS/NOAA-17	
	Dec06 Stderr (%)	Dec06 gain	Mar07 gain	Sep03 Stderr (%)	Jul04 Stderr (%)
0.65μm	5.6	0.6125	0.59	1.4	1.9
0.86μm	7.6	0.5126	0.45	3.5	4.2
1.6μm	5.0	0.0871	0.88		

Table 2. Provides the December 2006 Meteosat-8 visible gains and standard error based on Terra-MODIS, the corresponding EUMETSAT gains. Aqua-MODIS and NOAA-17 AVHRR standard errors are shown for comparison.
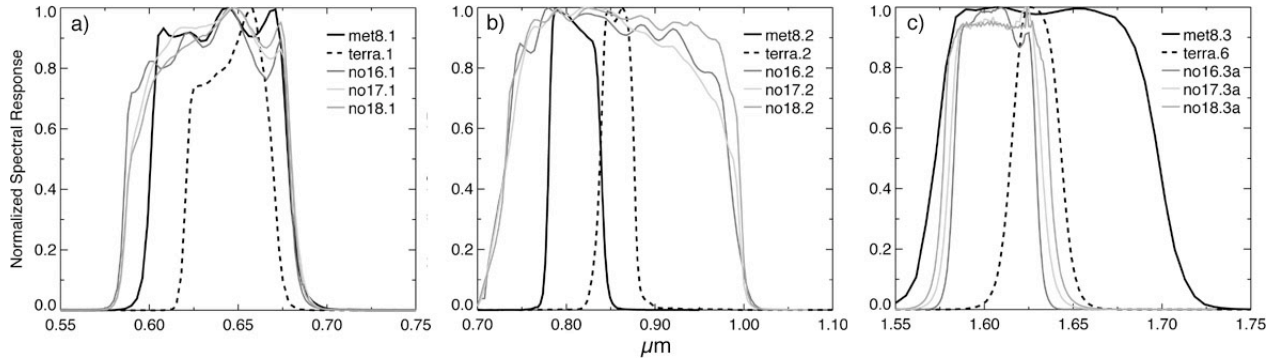
Figure 1a. Spectral response functions for Meteosat-8, Terra-MODIS, and NOAA-16 to 18, for the 0.65 µm visible channel. Figure 1b. Same as Figure 1a except for the 0.86 µm channel. Figure 1c. Same as Figure 1a except for the 1.6 µm channel.

2.2 Bilinear calibration methods

Four least squares statistical regression methods differing by the number and type of degrees of freedom allowed were developed to directly solve the gain and offset of both dual gains from multi-pixel FOV means where the means were stratified by the break point count. These methods work both for mixed gain FOV as well as for single gain FOV as long as both gains are represented. The NOAA-17 break points used are in Table 1. The mathematical equations are given in the appendix (A1-A4). The first method (4COF) predicts the gain and offset, where the dual gains are independent from each other, allowing a discontinuity at the break point and predicts the space count. The AVHRR/3 instrument incorporates a space clamp to use deep space as the space count (SC) offset to compute the radiance, which is kept constant. The SC is usually 40, however Ignatov et al. 2004 found that the in orbit SC may not equal the pre-launch SC and can drift ~0.2 counts over time. The second method (3SPC) forces the low gain regression through the SC. The third method (3COF) does not allow a discontinuity at the break point but predicts the SC. The fourth method does not allow a discontinuity and incorporates the SC. The fourth method (2COF) essentially only solves two unknowns, the two gains, which are mutually dependent. These methods rely on the fact that the break point is well known and does not change over time. Based on instrument engineering the break point only changes the amplification of the count to radiance conversion and the SC is constant, the method of choice is the 4th method. Since it has only two degrees of freedom, it is expected to have the most stable month-to-month calibration coefficient differences. The monthly gain changes would be interpreted as instrument gain degradation rather than oscillating coefficient noise due to compensating coefficient effects. However, if this approach is truly robust and AVHRR is a well-behaved instrument all 4 methods would reveal roughly the same calibration coefficients. Or these methods can be used to predict the "true" space count or more suitable breakpoint.

3. PRELIMINARY METEOSAT-8/NOAA-17 DUAL GAIN RESULTS

3.1 Results

Figure 2a shows a scatter plot of NOAA 17 0.65µm count means (using both low and high gain counts) and Meteosat-8 radiances of 865 regional coincident ray-matched points for February 2007. The black points indicate that the 95% of the regional pixel counts were either the low or high gain counts. The points near the break point are mainly gray points, where the count mean is taken from both high and low gain counts, and generally curve between the low and high gain slopes as expected. The NOAA-17 count dynamic range is greater than 800 almost the full extent. The dual slopes from the four methods are shown in gray-scale lines on the scatter plot and appear to be very similar. The regression coefficients are given in Table 3. All four methods computed low and high gains are within 3.0% and 0.7% respectively. The 3SPC and 2SPC gains, which have specified SC, are less than 0.2%. The 4COF and 3COF may suggest that the SC should be slightly higher. If the instrument was engineered to double the gain at the break-point, the four methods nearly all have a ratio of 3 between the high and low gains and is more consistent than the nominal gain ratio. The black dual slope is the nominal or pre-launch derived gain. The standard error using the 2SPC method is 4.67% and is very close to the standard error when using the nominal calibration and then comparing with Meteosat-8 radiances. The spectral response of Meteosat-8 and NOAA-17 are very similar in the 0.65µm channel. The nominal slope of 1.051, may suggest that the degradation from nominal calibration is on the order of 5%. This result is much less than the

Doelling et al. 2004 NOAA-17/Aqua-MODIS regression, which was based on 6 monthly points with incomplete seasonal cycles. However, it is more in line with the NOAA-16/Terra-MODIS degradation of 0.7%/year. These inconsistencies should be resolved by the August 2007 meeting. The AVHRR pixel radiances are derived from GAIN and Coff as follows:

If C > breakpoint, Radiance (Wm-2str-1um-1) = Gain2 *(C + Coff2) or
If C < breakpoint, Radiance (Wm-2str-1um-1) = Gain1 *(C + Coff1)

Similar consistencies between methods for the other channels can be stated. However the differences between the 2SPC and nominal gains are considerable. It is not known what the cause is, certainly spectral differences play a role, as the standard errors are much larger. To determine whether spectral differences play a role, this analysis should be applied soon after launch to isolate spectral changes from degradation over time. Note that the MODIS 0.86µm saturates.
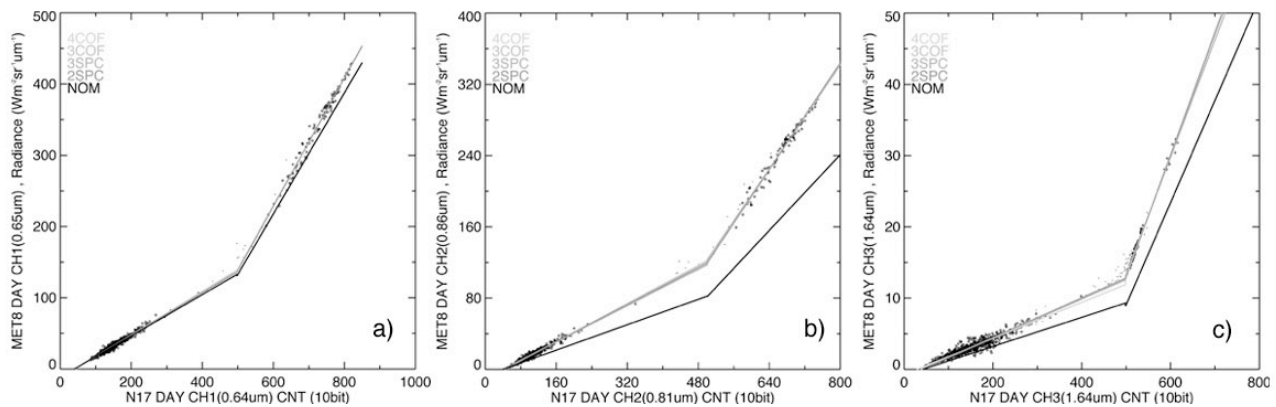

Figure 2a. Scatter plot of the NOAA-17 regional mean counts with the Meteosat-8 regional radiances for the 0.65µm channel. The 4 method regression gains are explained in section 2.1 and nominal gain is also plotted on the scatter plot. Figure 2b is the same as Figure 2a except for the 0.86µm channel. Figure 2c is the same as Figure 2a except for the 1.6µm channel

NOAA-17 Channel Feb07	Gain/ Coff	4COF	3COF	3SPC	2SPC	NOM	2SPC stderr (%), #	NOM stderr (%) slope
0.65µm	Gain1	0.3064	0.3020	0.2973	0.2974	0.29	4.67	4.65
	Coff1	-44.02	-42.55	-40.0	-40.0	-40.0	865	1.051
	Gain2	0.9011	0.8952	0.8992	0.9007	0.85		
	Coff2	-346.0	-344.0	-345.8	-346.4	-344.0		
0.86µm	Gain1	0.2661	0.2675	0.2553	0.2598	0.1783	6.00	6.13
	Coff1	-43.68	-43.98	-40.0	-40.0	-40.0	865	1.440
	Gain2	0.7340	0.7363	-0.7300	0.7504	0.5323		
	Coff2	-333.4	-334.5	-331.5	-341.0	-346.8		
1.6µm	Gain1	0.0253	0.0275	0.274	0.279	0.0204	9.46	10.44
	Coff1	-28.70	-37.35	-40.0	-40.0	-40.0	865	1.33
	Gain2	0.1636	0.1724	0.1646	0.1704	0.1434		
	Coff2	-417.9	-425.1	-419.0	-423.6	-436.8		

Table 3. Provides the dual gains and count offsets (Coff) for both less than the breakpoint (Gain1) and greater than the break point and can be used in the above equation for all 4 dual regression methods outlined in section 2.2. The second column on the right shows the standard error of the 2SPC method and the number of points used in the regression. The column on the right shows the standard error if using the nominal or pre-launch coefficients and resultant slope when regressed against the Meteosat-8 radiances.

4. EFFECTS OF MIXED COUNT FOV IN THE 4 METHODS

4.1 Results

The results from section 3 did not include many well-mixed FOV in the scatter plots, because the spatial homogeneity test in section 2.1 limited those regions. A regional standard deviation of 20% was used for a threshold. The four methods are designed to work with mixed count regions or single count regions of both gains. To test the robustness of the four methods under mixed conditions the spatial coherence test was not used. Figure 3a shows the scatter plot with lines representing each of the 4 regression methods. Table 4 shows the results under "all regions" for the 0.65μm channel. Note that the gains and offsets are similar within 2-3%, however the standard error of the 2PSC fit doubled to 9.4%. The black points are those where the 95% of the pixels are of one count and the gray points are the rest. All the regions, which have pixels of the same count that are greater than 97%, are removed and the resultant plot is shown in Figure 3b. This leaves 659 points out of the original 1993. Table 4 shows that the "Mixed region" gain and offsets again are very similar to the "All region" coefficients. Note that the standard error of the 2SPC regression increased only slightly, which validates the robustness of the method.
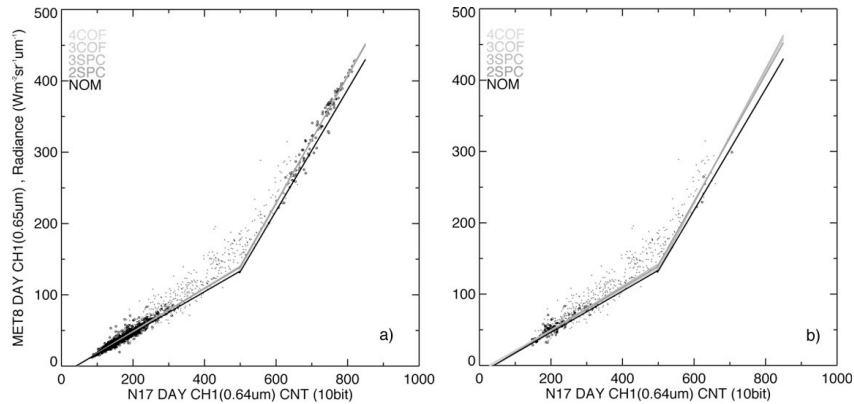

Figure 3a is the same as Figure 2a except for the spatial coherence test was not used. Figure 3b is the same as Figure 3a except for only mixed regions as define in section 4.1 were used.

0.65μm Feb07	Gain/ Coff	4COF	3COF	3SPC	2SPC	NOM	2SPC stderr (%), #	NOM slope
All regions	Gain1	0.3078	0.3010	0.3036	0.3017	0.29	9.4	9.4
	Coff1	-42.40	-39.82	-40.0	-40.0	-40.0	1993	1.051
	Gain2	0.9018	0.8885	0.8991	0.8871	0.85		
	Coff2	-348.1	-342.5	-346.9	-341.9	-344.0		
Mixed regions	Gain1	0.2949	0.2883	0.3090	0.3029	0.29	10.3	10.3
	Coff1	-31.06	-27.45	-40.0	-40.0	-40.0	659	1.052
	Gain2	0.9312	0.9139	0.9427	0.8906	0.85		
	Coff2	-355.0	-349.3	-359.0	-341.9	-344.0		

Table 4. Is the same as Table 3 except that the difference between mixed count regions and all regions with no spatial coherence test are shown for the 0.65μm channel.

5. CONCLUSIONS AND FUTURE WORK

Four regression methods were developed to handle dual gains for spatial regions that contain pixel counts from both gains. The regressions simultaneously derive both gains and offsets. The four methods provided consistent gains and offsets with each other under differing spatial coherence restrictions, which essentially defines the number of mixed regions in the analysis, for all visible channels. This validates the robustness of the methods in using the information from all regions. The standard errors of the regression were as good as the nominal coefficients or better. These methods will be validated with a complete timeline of NOAA/Meteosat-8, Meteosat-8/MODIS, NOAA-AM/NOAA-PM, and

NOAA/MODIS regression at the poles. If the methods are robust they can be incorporated operationally such as for the CLARREO mission to determine the degradation of dual gain instruments.

REFERENCES

1. Abel, P. and B. Guenther, 1993; Calibration results for NOAA-11 AVHRR Channels 1 and 2 from congruent path aircraft observations. *J. Atmos. Ocean. Technol.* **10**, 493-508.
2. Doelling, D. R., V. Chakrapani, P. Minnis, L. Nguyen, 2001: The Calibration of NOAA-AVHRR Visible Radiances with VIRS. *Proc. AMS 11th Conf. Atmos. Radiation*, Madison, WI, Oct 15 –18.
3. Doelling, D.R., L. Nguyen, P. Minnis, 2004, On the use of deep convective clouds to calibrate AVHRR data. *Proc. SPIE 49th Ann. Mtg., Earth Observing Systems IX Conf., Denver, CO, August 2-6.*
4. Heidinger, A.K., C Cao,, J.T. Sullivan, 2002: Using Moderate Resolution Imaging Spectrometer (MODIS) to calibration advanced resolution radiometer reflectance channels. *J. of Geophysical Research*, Vol. **107**, No D23, 4702, doi:10.1029/2001JD002035.
5. Hu, Y**.,** B. Wielicki, P. Yang, P. Stackhouse, B. Lin, and D. Young, 2004: Application of Deep Convective Cloud Albedo Observation to Satellite-based Study of Terrestrial Atmosphere: Monitoring Stability of Space-borne Measurements and Assessing Absorption Anomaly, *IEEE Trans. Geosci. Remote Sensing* (accepted).
6. Ignatov, A., C. Cao, J. Sullivan, R. Levin, X. Wu, R. Galvin, 2004: The Usefulness of In-Flight Measurements of Space Count to Improve Calibration of the AVHRR Solar Reflectance Bands, *J. Atmos. Ocean. Technol.* **22**, 180-200.
7. Loeb, N. G., 1997: In-flight calibration of NOAA AVHRR visible and near-IR bands over Greenland and Antarctica. *Intl Jour. Remote Sens.*, **18**, 477-490.
8. Minnis, P., D.R. Doelling, L. Nguyen, W.F. Miller, 2007a. Assessment of the Visible Channel Calibrations of the VIRS on TRMM and MODIS on Aqua and Terra. *J. Atmospheric and Oceanic Technology* (accepted).
9. Minnis, P., L. Nguyen, and D.R.Doelling, 2007b. Calibration of Satellite Imager Channels Using Inter-Satellite Normalization and Deep Convective Cloud Targets. 1st meeting Global Space-Based Inter-Satellite Calibration System (GSICS) Research Working Group (GRWG-1), Camp Springs, MD, Jan 22-23, 2007 (http://www.orbit.nesdis.noaa.gov/smcd/spb/calibration/icvs/GSICS/index.html)
10. Minnis, P., L. Nguyen, D. R. Doelling, D. F. Young, W. F. Miller, 2001: Rapid Calibration Calibration of Operation and Research Meteorological Satellite Imagers, Part I: Use of the TRMM VIRS or ERS-2 ATSR-2 as a Reference. *J. Atmos. Ocean. Technol.* **19**, 1233-1249.
11. Nguyen, L., D. R. Doelling, P. Minnis, and J. K. Ayers 2004: Rapid Technique to cross calibrate satellite imager with visible channels *Proc. of 49th SPIE Meeting, Denver, CO, Aug. 2-6, 2004.*
12. Rao, C. R. N., and J. Chen, 1999: Revised post-launch calibration of the visible and near-infrared channels of the Advanced Very High Resolution Radiometer on the NOAA-14 spacecraft. *Intl Jour. Remote Sens.*, **20**, 3485-3491
13. Wielicki, B.A., et al. 2007: CLARREO as "NIST in Orbit". *CLARREO Workshop*, Adelphi, MD, July 17-19, 2007, (http://map.nasa.gov/clarreo_presentations.html)

Appendix: Bilinear Calibration Methods

For some region i, calculate separate statistics for those counts that fall below and those that fall above the threshold c_t of a sensor with bilinear characteristic

$$\bar{c}_{bi} = \frac{1}{n_b} \sum_{j=1}^{n_b} (c_j - c_t) \qquad\qquad , c_j \leq c_t$$

$$\bar{c}_{ai} = \frac{1}{n_a} \sum_{j=1}^{n_a} (c_j - c_t) \qquad\qquad , c_j > c_t$$

The fractions of samples in region i below and above the threshold are

$$f_{bi} = \frac{n_b}{n_a + n_b}$$

$$f_{ai} = \frac{n_a}{n_a + n_b}$$

and an estimate of the radiance for the region is

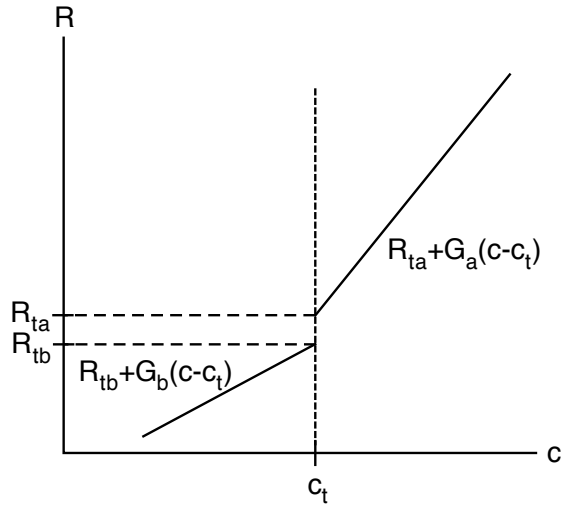$$R_i = f_{bi} R_{bi} + f_{ai} R_{ai}$$

where the conversion from counts to radiance below and above the threshold may take on a number of different forms.

Discontinuous Method without Space Count

For this method the conversions from counts to radiance below and above the threshold are linear, distinct, and discontinuous

$$R_{bi} = R_{tb} + G_b \bar{c}_{bi}$$
$$R_{ai} = R_{ta} + G_a \bar{c}_{ai}$$

with R_{ta}, G_a, R_{tb}, and G_b parameters to be determined. If there is another estimate of radiance for

the region, D_i, from another satellite the difference (or error) between the two estimates is given by

$$\epsilon_i = R_i - D_i = f_{bi}(R_{tb} + G_b \bar{c}_{bi}) + f_{ai}(R_{ta} + G_a \bar{c}_{ai}) - D_i$$

The sum of the squared differences (or errors) over all m regions

$$E = \sum_{i=1}^{m} \epsilon_i^2$$

is minimized by setting the partial derivative of each of the parameters equal to zero. The partial of E with respect to some parameter p is

$$\frac{\partial E}{\partial p} = 2 \sum_{i=1}^{m} \epsilon_i \frac{\partial \epsilon_i}{\partial p}$$

where partials for each of the parameters are

$$\frac{\partial \epsilon_i}{\partial R_{tb}} = f_{bi}$$

$$\frac{\partial \epsilon_i}{\partial G_b} = f_{bi} \bar{c}_{bi}$$

$$\frac{\partial \epsilon_i}{\partial R_{ta}} = f_{ai}$$

$$\frac{\partial \epsilon_i}{\partial G_a} = f_{ai} \bar{c}_{ai}$$

This gives

$$0 = \sum_{i=1}^{m} \{(f_{bi}(R_{tb} + G_b \bar{c}_{bi}) + f_{ai}(R_{ta} + G_a \bar{c}_{ai})) - D_i\} f_{bi}$$

$$0 = \sum_{i=1}^{m} \{(f_{bi}(R_{tb} + G_b \bar{c}_{bi}) + f_{ai}(R_{ta} + G_a \bar{c}_{ai})) - D_i\} f_{bi} \bar{c}_{bi}$$

$$0 = \sum_{i=1}^{m} \{(f_{bi}(R_{tb} + G_b \bar{c}_{bi}) + f_{ai}(R_{ta} + G_a \bar{c}_{ai})) - D_i\} f_{ai}$$

$$0 = \sum_{i=1}^{m} \{(f_{bi}(R_{tb} + G_b \bar{c}_{bi}) + f_{ai}(R_{ta} + G_a \bar{c}_{ai})) - D_i\} f_{ai} \bar{c}_{ai}$$

which can be solved for the intercepts, R_{tb} and R_{ta}, and gains, G_b and G_a,

$$\begin{pmatrix} \sum f_b^2 & \sum f_b^2 \bar{c}_b & \sum f_b f_a & \sum f_b f_a \bar{c}_a \\ \sum f_b^2 \bar{c}_b & \sum f_b^2 \bar{c}_b^2 & \sum f_b f_a \bar{c}_b & \sum f_b f_a \bar{c}_b \bar{c}_a \\ \sum f_b f_a & \sum f_b f_a \bar{c}_b & \sum f_a^2 & \sum f_a^2 \bar{c}_a \\ \sum f_b f_a \bar{c}_a & \sum f_b f_a \bar{c}_b \bar{c}_a & \sum f_a^2 \bar{c}_a & \sum f_a^2 \bar{c}_a^2 \end{pmatrix}$$

$$\times \begin{pmatrix} R_{tb} \\ G_b \\ R_{ta} \\ G_a \end{pmatrix} = \begin{pmatrix} \sum f_b D \\ \sum f_b D \bar{c}_b \\ \sum f_a D \\ \sum f_a D \bar{c}_a \end{pmatrix}$$

so that the equation for radiance is now given by

$$R_i = f_{bi}(R_{tb} + G_b \bar{c}_{bi}) + f_{ai}(R_{ta} + G_a \bar{c}_{ai})$$

The two lines defining the calibration curve are then

$$R = R_{tb} + G_b(c - c_t) \qquad , c < c_t$$
$$= R_{ta} + G_a(c - c_t) \qquad , c > c_t$$

which poses a problem for interpretating either of the two possibilities arising if $R_{tb} \neq R_{ta}$. In either case an estimate of the space count is

$$\hat{c}_s = c_t - \frac{R_{tb}}{G_b}$$

If there are no regions in which there are counts both above and below the threshold, then $f_a f_b = 0$ and the fits above and below the threshold uncouple

$$\begin{pmatrix} m_b & \sum \bar{c}_b \\ \sum \bar{c}_b & \sum \bar{c}_b^2 \end{pmatrix} \begin{pmatrix} R_{tb} \\ G_b \end{pmatrix} = \begin{pmatrix} \sum D \\ \sum D\bar{c}_b \end{pmatrix}$$
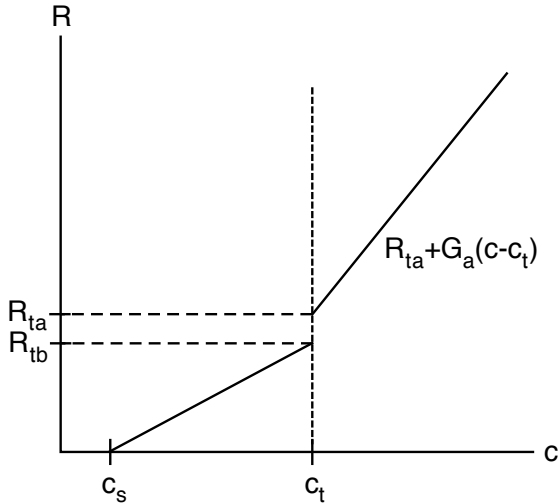
$$\begin{pmatrix} m_a & \sum \bar{c}_a \\ \sum \bar{c}_a & \sum \bar{c}_a^2 \end{pmatrix} \begin{pmatrix} R_{ta} \\ G_a \end{pmatrix} = \begin{pmatrix} \sum D \\ \sum D\bar{c}_a \end{pmatrix}$$

Discontinuous Method with Space Count
For this method the conversions from counts to radiance below and above the threshold are linear, distinct, and discontinuous but the line below the threshold is pegged to a known space count

$$R_{bi} = R_{tb} \left(1 + \frac{\bar{c}_{bi}}{c_t - c_s} \right) = R_{tb} \gamma_i$$
$$R_{ai} = R_{ta} + G_a \bar{c}_{ai}$$

where c_s is the space count. Parameters R_{ta}, G_a, and R_{tb} are to be determined and $\gamma_i = 1 + \bar{c}_{bi}/(c_t - c_s)$ is used just to simplify the notation. If there is another estimate of radiance for the region, D_i, from

another satellite the difference (or error) between the two estimates is given by

$$\epsilon_i = R_i - D_i = f_{bi} R_{tb} \gamma_i + f_{ai}(R_{ta} + G_a \bar{c}_{ai}) - D_i$$

As before, the sum of the squared differences (or errors) over all m regions is minimized by setting the partial derivative of each of the parameters equal to zero. The partials for each of the parameters are

$$\frac{\partial \epsilon_i}{\partial R_{tb}} = f_{bi} \gamma_i$$
$$\frac{\partial \epsilon_i}{\partial R_{ta}} = f_{ai}$$
$$\frac{\partial \epsilon_i}{\partial G_a} = f_{ai} \bar{c}_{ai}$$

This gives

$$0 = \sum_{i=1}^{m} \{f_{bi} R_{tb} \gamma_i + f_{ai}(R_{ta} + G_a \bar{c}_{ai}) - D_i\} f_{bi} \gamma_i$$

$$0 = \sum_{i=1}^{m} \{f_{bi} R_{tb} \gamma_i + f_{ai}(R_{ta} + G_a \bar{c}_{ai}) - D_i\} f_{ai}$$

$$0 = \sum_{i=1}^{m} \{f_{bi} R_{tb} \gamma_i + f_{ai}(R_{ta} + G_a \bar{c}_{ai}) - D_i\} f_{ai} \bar{c}_{ai}$$

which can be solved for the intercepts, R_{tb} and R_{ta}, and gain, G_a,

$$\begin{pmatrix} \sum f_b^2 \gamma^2 & \sum f_b f_a \gamma & \sum f_b f_a \gamma \bar{c}_a \\ \sum f_b f_a \gamma & \sum f_a^2 & \sum f_a^2 \bar{c}_a \\ \sum f_b f_a \gamma \bar{c}_a & \sum f_a^2 \bar{c}_a & \sum f_a^2 \bar{c}_a^2 \end{pmatrix} \begin{pmatrix} R_{tb} \\ R_{ta} \\ G_a \end{pmatrix}$$
$$= \begin{pmatrix} \sum f_b D \gamma \\ \sum f_a D \\ \sum f_a D \bar{c}_a \end{pmatrix}$$

so that the equation for radiance is now given by

$$R_i = f_{bi} R_{tb} \left(1 + \frac{\bar{c}_{bi}}{c_t - c_s} \right) + f_{ai}(R_{ta} + G_a \bar{c}_{ai})$$

The two lines defining the calibration curve are then

$$R = R_{tb} \left(\frac{c - c_s}{c_t - c_s} \right) \qquad , c_s \leq c < c_t$$
$$= R_{ta} + G_a(c - c_t) \qquad , c > c_t$$

which again poses a problem for interpretating either of the two possibilities arising if $R_{tb} \neq R_{ta}$. In either case the gain for the region below the threshold is simply

$$G_b = \frac{R_{tb}}{c_t - c_s}$$

A2

If there are no regions in which there are counts both above and below the threshold, then $f_a f_b = 0$ and the fits above and below the threshold uncouple
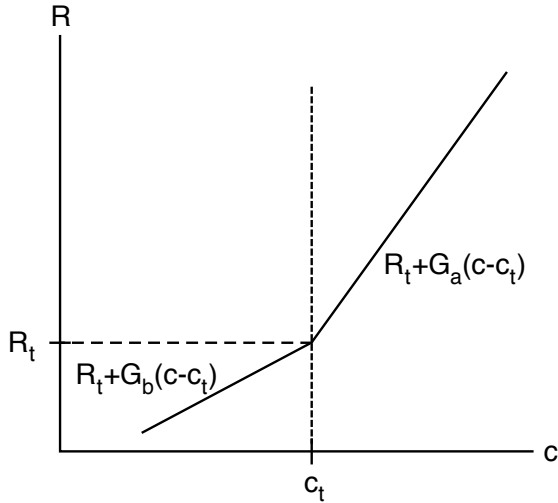
$$R_{tb} = \frac{\sum \gamma D}{\sum \gamma^2}$$

$$\begin{pmatrix} m_a & \sum \bar{c}_a \\ \sum \bar{c}_a & \sum \bar{c}_a^2 \end{pmatrix} \begin{pmatrix} R_{ta} \\ G_a \end{pmatrix} = \begin{pmatrix} \sum D \\ \sum D\bar{c}_a \end{pmatrix}$$

Continuous Method without Space Count

For this method the conversions from counts to radiance below and above the threshold are linear and distinct but continuous

$$R_{bi} = R_t + G_b \bar{c}_{bi}$$
$$R_{ai} = R_t + G_a \bar{c}_{ai}$$

with G_b, G_a, and R_t parameters to be determined. If there is another estimate of radiance for the region, D_i, from another satellite the difference (or error) between the two estimates is given by

$$\epsilon_i = R_i - D_i = R_t + G_b(f_{bi}\bar{c}_{bi}) + G_a(f_{ai}\bar{c}_{ai}) - D_i$$

This can be simplified by defining new variables

$$\beta_i = f_{bi}\bar{c}_{bi} = \frac{1}{n_b + n_a} \sum_{j=1}^{n_b} (c_j - c_t) \qquad , c_j \le c_t$$

$$\alpha_i = f_{ai}\bar{c}_{ai} = \frac{1}{n_b + n_a} \sum_{j=1}^{n_a} (c_j - c_t) \qquad , c_j > c_t$$

so that the error equation is now

$$\epsilon_i = R_i - D_i = R_t + G_b\beta_i + G_a\alpha_i - D_i$$

The sum of the squared differences (or errors) over all m regions is minimized by setting the partial derivative of E with respect to each of the parameters equal to zero. The partials for each of the parameters are

$$\frac{\partial \epsilon_i}{\partial R_t} = 1$$
$$\frac{\partial \epsilon_i}{\partial G_b} = \beta_i$$
$$\frac{\partial \epsilon_i}{\partial G_a} = \alpha_i$$

This gives

$$0 = \sum_{i=1}^{m} \{(R_t + G_b\beta_i + G_a\alpha_i) - D_i\}$$

$$0 = \sum_{i=1}^{m} \{(R_t + G_b\beta_i + G_a\alpha_i) - D_i\}\beta_i$$

$$0 = \sum_{i=1}^{m} \{(R_t + G_b\beta_i + G_a\alpha_i) - D_i\}\alpha_i$$

which can be solved for the gains, G_b and G_a, and radiance threshold, R_t

$$\begin{pmatrix} m & \sum \beta & \sum \alpha \\ \sum \beta & \sum \beta^2 & \sum \beta\alpha \\ \sum \alpha & \sum \beta\alpha & \sum \alpha^2 \end{pmatrix} \begin{pmatrix} R_t \\ G_b \\ G_a \end{pmatrix} = \begin{pmatrix} \sum D \\ \sum D\beta \\ \sum D\alpha \end{pmatrix}$$

and the equation for radiance is now given by

$$R_i = R_t + G_b\beta_i + G_a\alpha_i$$

The two lines defining the calibration curve are then

$$R = R_t + G_b(c - c_t) \qquad , c \le c_t$$
$$= R_t + G_a(c - c_t) \qquad , c > c_t$$

and an estimate of the space count is then

$$\hat{c}_s = c_t - \frac{R_t}{G_b}$$

Continuous Method with Space Count

For this method the conversions from counts to radiance below and above the threshold are linear, distinct, and continuous but the line below the threshold is pegged to a known space count
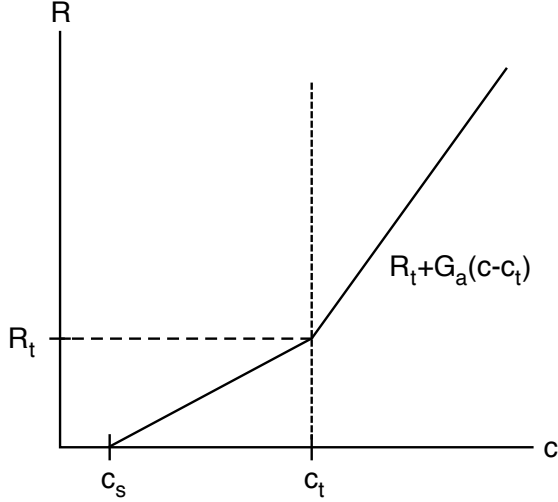
$$R_{bi} = R_t \left(1 + \frac{\bar{c}_{bi}}{c_t - c_s}\right)$$
$$R_{ai} = R_t + G_a \bar{c}_{ai}$$

where c_s is the space count. G_a and R_t are parameters to be determined. If there is another estimate

of radiance for the region, D_i, from another satellite the difference (or error) between the two estimates is given by

$$\epsilon_i = R_i - D_i = R_t \left(1 + \frac{f_{bi}\bar{c}_{bi}}{c_t - c_s}\right) + G_a\left(f_{ai}\bar{c}_{ai}\right) - D_i$$

This can be simplified by defining new variables

$$\beta_i = f_{bi}\bar{c}_{bi} = \frac{1}{n_b + n_a}\sum_{j=1}^{n_b}(c_j - c_t) \qquad , c_j \leq c_t$$

$$\alpha_i = f_{ai}\bar{c}_{ai} = \frac{1}{n_b + n_a}\sum_{j=1}^{n_a}(c_j - c_t) \qquad , c_j > c_t$$

so that the error equation is now

$$\epsilon_i = R_i - D_i = R_t \left(1 + \frac{\beta_i}{c_t - c_s}\right) + G_a\alpha_i - D_i$$
$$= R_t\xi_i + G_a\alpha_i - D_i$$

where $\xi_i = 1 + \beta_i/(c_t - c_s)$ is used just to simplify the notation. The sum of the squared differences (or errors) over all m regions is minimized by setting the partial derivative of each of the parameters equal to zero. The partials for each of the parameters are

$$\frac{\partial \epsilon_i}{\partial R_t} = \xi_i$$

$$\frac{\partial \epsilon_i}{\partial G_a} = \alpha_i$$

This gives

$$0 = \sum_{i=1}^{m}\{R_t\xi_i + G_a\alpha_i - D_i\}\xi_i$$

$$0 = \sum_{i=1}^{m}\{R_t\xi_i + G_a\alpha_i - D_i\}\alpha_i$$

which can be solved for the gain, G_a and the radiance threshold, R_t

$$\left(\begin{array}{cc} \sum \xi^2 & \sum \xi\alpha \\ \sum \xi\alpha & \sum \alpha^2 \end{array}\right)\left(\begin{array}{c} R_t \\ G_a \end{array}\right) = \left(\begin{array}{c} \sum D\xi \\ \sum D\alpha \end{array}\right)$$

and the equation for radiance is now given by

$$R_i = R_t \left(1 + \frac{\beta_i}{c_t - c_s}\right) + G_a\alpha_i$$

The two lines defining the calibration curve are then

$$R = R_t\left(\frac{c - c_s}{c_t - c_s}\right) \qquad\qquad , c_s \leq c \leq c_t$$
$$= R_t + G_a(c - c_t) \qquad\qquad , c > c_t$$

The gain for the region below the threshold is simply

$$G_b = \frac{R_t}{c_t - c_s}$$